SCIENCE CHINA
Chemistry

• ARTICLES •

January 2016 Vol.59 No.1: 142–149
doi: 10.1007/s11426-015-5438-2

ZnO nanopowders and their excellent solar light/UV photocatalytic activity on degradation of dye in wastewater

Yingying Lv, Leshu Yu*, Chungen Li & Liusai Yang

School of Chemistry and Chemical Engineering, Shangrao Normal University, Shangrao 334001, China

Received February 28, 2015; accepted March 18, 2015; published online June 10, 2015

Low-cost and scalable preparation, high photocatalytic activity, and convenient recycle of ZnO nanopowders (NPs) would determine their practical application in purifying wastewater. In this contribution, ZnO NPs were scalably synthesized via the simple reaction of Zn powder with H_2O vapor in autoclave. The structural, morphological and optical properties of the samples were systematically characterized by X-ray diffraction, scanning electron microscopy, Fourier transform infrared spectra, transmission electron microscopy, Micro-Raman, photoluminescence, and ultraviolet-visible spectroscopy. The as-prepared ZnO NPs are composed of nanoparticles with 100–150 nm in diameter, and have a small Brunauer-Emmett-Teller surface area of 6.85 m^2/g. The formation of ZnO nanoparticles is relative to the peeling of H_2 release. Furthermore, the product has big strain-stress leading to the red-shift in the band gap of product, and shows a strong green emission centered at 515 nm revealing enough atomic defects in ZnO NPs. As a comparison with P25, the obtained dust gray ZnO NPs have a strong absorbance in the region of 200–700 nm, suggesting the wide wave-band utilization in sunlight. Based on the traits above, the ZnO NPs show excellent photocatalytic activity on the degradation of rhodamine B (Rh-B) under solar light irradiation, close to that under UV irradiation. Importantly, the ZnO NPs could be well recycled in water due to the quick sedimentation in themselves in solution. The low-cost and scalable preparation, high photocatalytic activity, and convenient recycle of ZnO NPs endow themselves with promising application in purifying wastewater.

ZnO nanopowders, Zn powder, photocatalyst, solar light, degradation

Citation: Lv YY, Yu LS, Li CG, Yang LS. ZnO nanopowders and their excellent solar light/UV photocatalytic activity on degradation of dye in wastewater. *Sci China Chem*, 2016, 59: 142−149, 10.1007/s11426-015-5438-2

1 Introduction

Environmental pollution derived from urbanization and heavy industrialization is a global menace to man's health, and the magnitude of it is increasing day by day. Especially, wastewater released from chemical industries is one of the main pollution sources because it has high concentration of large organic molecules which are extremely toxic and carcinogenic in nature. So far the environmental remediation technologies, including adsorption, biological oxidation, chemical oxidation, and incineration, have been used to treat all types of organic and toxic wastewater; therein one of the typical environmental remediation methods is chemical degradation. In chemical degradation methods, photocatalytic degradation involving photons and a catalyst is widely used to treat organic wastewater [1]. Therefore, developing solar light-driven photocatalysts is the optimal treatment for organic wastewater.

To date, many photocatalytic nanomaterials, including metal oxides, metal sulfides, metal nitrides, heterojunction nanocomposites, oxynitrides, oxysulfides, and graphitic carbon nitride, have been exploited to actualize the photocatalytic degradation of organic pollutants in wastewater

*Corresponding author (email: yuleshu2008@126.com)

[2–4]. However, most reported photocatalysts have some evident disadvantages such as high cost, small scale, low photocatalytic activity, and difficult recycle, which determine their unpractical applications in wastewater. Comparatively speaking, TiO_2- and ZnO-based nanomaterials show the most promising applications in environmental remediation field due to their low cost, high photocatalytic activity and no second pollution [5,6]. For example, Degussa P25, a typical and commercially applied TiO_2 product, has so far been most extensively used, and has become a worldwide reference in lab. However, the P25 preparation, realized via the combustion of $TiCl_4$ in O_2/H_2 mixed atmosphere, leads to acid mist and fouls the ambient. Furthermore, P25 has some other characteristics such as small density, small size, porous structure, and good suspension in water. Hence, it is difficult to recover P25 from water, limiting its further extensive application in wastewater. ZnO is also an ideal photocatalyst because of its band gap close to TiO_2, nontoxicity, and abundance. Also, ZnO has some other evident advantages in the sense that it absorbs over a larger fraction of UV spectrum and has lower preparation cost in contrast to TiO_2 [7]. Therefore, low-cost and scalable preparation, high photocatalytic activity, and convenient recycle of ZnO nanopowders (NPs) would be of significance, which determines their practical application in purifying wastewater.

ZnO NPs were preferentially prepared via wet chemical routes due to the simple, less expensive, high yielding, and scalable process, in which some Zn-containing salts were decomposed in liquid-phase reactions [8]. However, the obtained products suffered from either low photocatalytic activity or difficult recycle, probably owing to small size, porous structure and low crystalline degree of nanoparticles. As known, these features usually lead to photocorrosion and fast electron-hole recombination [9–13]. Very recently, some new techniques such as coating or doping with transition metal ions have been developed to delay photocorrosion and prevent fast electron-hole recombination [14,15]. However, these additional operations would have to increase the cost of ZnO-based photocatalysts, and ultimately limit their practical application in wastewater. In our previous report, ZnO NPs were cheaply and scalably prepared by the soluble salt-assisted route via the simple oxidation of Zn-Na_2SO_4 mixture, and the as-prepared products showed high efficiency and good recycle on the degradation of rhodamine B (RhB) [16]. In this study, ZnO NPs were scalably synthesized via the simple reaction between Zn powder and H_2O vapor in autoclave. The as-prepared products are composed of nanoparticles with 100–150 nm in diameter, and show excellent photocatalytic activity on the degradation of RhB under solar light irradiation. On comprehensively balancing all issues of ZnO NPs, such as low-cost and scalable preparation, high photocatalytic activity, and convenient recycle, the as-synthesized ZnO NPs have promising application in purifying waste water.

2 Experimental

2.1 Materials preparation

The schematic diagram of preparation set up is shown in Figure 1. Namely, 5.000 g of zinc powder (steel gray, 99.99%, 200 mesh, seen in Figure S1, Supporting Information online) and a weighing bottle filled with 10 mL H_2O were put into a 100 mL teflon-lined autoclave. The autoclave was sealed and maintained at 230 °C for 10 h in oven and then cooled to room temperature naturally. Finally, the product was dried in an oven at 80 °C for 3 h and 6.043 g of dusty gray powder was obtained. The yield of ZnO was ca. 97%, based on the amount of Zn powder used. The little loss of the product is from the transferring process.

2.2 Materials characterization

The product was systematically characterized by scanning electron microscopy (SEM, JEOL JSM-6300, Japan), X-ray diffraction (XRD, Philips X'pert Pro diffractometer, Japan), Fourier transform infrared spectra (FT-IR, Nicolet Magna 560 FT-IR spectrometer, USA, at a resolution of 2 cm^{-1}), field emission gun transmission electron microscope (TEM, JEOL JEM 2100F, Japan) equipped with energy-dispersive X-ray analysis (EDX), Brunauer-Emmett-Teller (BET) surface area (Micromeritics ASAP 2020, USA), micro-Raman spectroscopy (excited with an Ar^+ laser at 488 nm), photoluminescence spectrum (PL, Bowman Series-2 spectrometer, Amino, USA, excited with a Xe^+ line at 294 nm) and ultraviolet-visible (UV-Vis) diffuse reflectance spectra (VARIAN Cary-5000 UV/Vis/NIR spectrophotometer, USA).

2.3 Photocatalytic activity of the synthesized materials

The photocatalytic activity of ZnO samples was evaluated by the photodegradation of rhodamine B (Rh-B) aqueous solution with an initial concentration of 12 mg/L, and compared with P25 under the same condition. Herein solar light was used as the preferential light source and a 36 W mer-

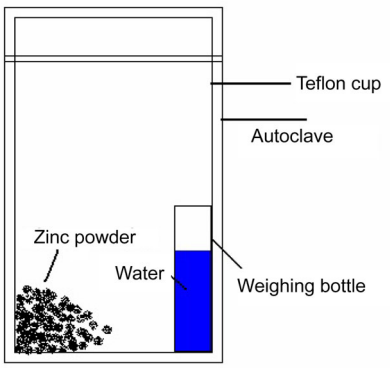

Figure 1 Schematic diagram of preparation set-up.

cury lamp (λ=365 nm) was used sometimes for a consulted UV light source. The sunlight experiments were carried out between 10:00 a.m. and 14:00 p.m. during the days of January (environment temperature is in range of 0–5 °C) at Shangrao City. Unless otherwise noted, 50 mg of catalyst powder was added to 35 mL of Rh-B solution in a quartz cup, corresponding to a catalyst dosage of 1.4 g/L. Before solar irradiation, the whole system was placed in the dark for 30 min to ensure an adsorption/desorption equilibrium. At given time intervals, about 2 mL aliquots were sampled, and centrifuged. Then, the top clear solution was analyzed by recording variations in the absorption in UV-Vis spectra of Rh-B. According to the standard curve between concentration and absorption, the value of $(1-C/C_0)$ was calculated, which is denoted as the degradation ratio.

3 Results and discussion

3.1 Morphological observations and structural analysis of the photocatalyst

3.1.1 SEM images, XRD pattern, and FT-IR spectrum

Figure 2(a, b) shows the SEM images of the dust gray product. It is seen that many nanoparticles with the mean size of several hundred nanometers in diameter were congregated to form a large particulate. Also, the sizes of ZnO NPs particulates correspond to the size of primal Zn powder (Figure S1), indicating most original Zn particulates did not break up thoroughly into many individuals after undergoing the poignant reaction with water in autoclave. Figure 2(c) is the XRD pattern of the product, and the strident peaks reveal the wurtzite ZnO phase and high crystalline degree of ZnO NPs. As a comparison with our previous ZnO NPs, the size and crystalline degree of ZnO NPs in this contribution are larger and higher [16], which might delay photocorrosion and suppress electron-hole recombination, and ultimately enhance the photocatalytic activity [9–13]. Herein, ZnO NPs were synthesized via the simple reaction of Zn powder with water: $Zn+H_2O=ZnO+H_2\uparrow$. The release of H_2 played a key role of peeling newly formed ZnO nanoparticles from micrometers-sized Zn matrix. Thus the latter reaction could successfully go along. If there is no release of gas, the new formed ZnO may cover Zn particulate, and inhibit the latter reaction. For instance, heating micrometer-sized Zn powder in air at 700 °C could not harvest ZnO powder in our previous report just because of no release of gas during the reaction: $2Zn+O_2=2ZnO$ [16]. Since the releasing rate of H_2 is uncontrollable in this reaction, the final ZnO nanoparticles are irregular, and their sizes are varied. Figure 2(d) shows a typical FT-IR spectrum of as-formed ZnO NP.

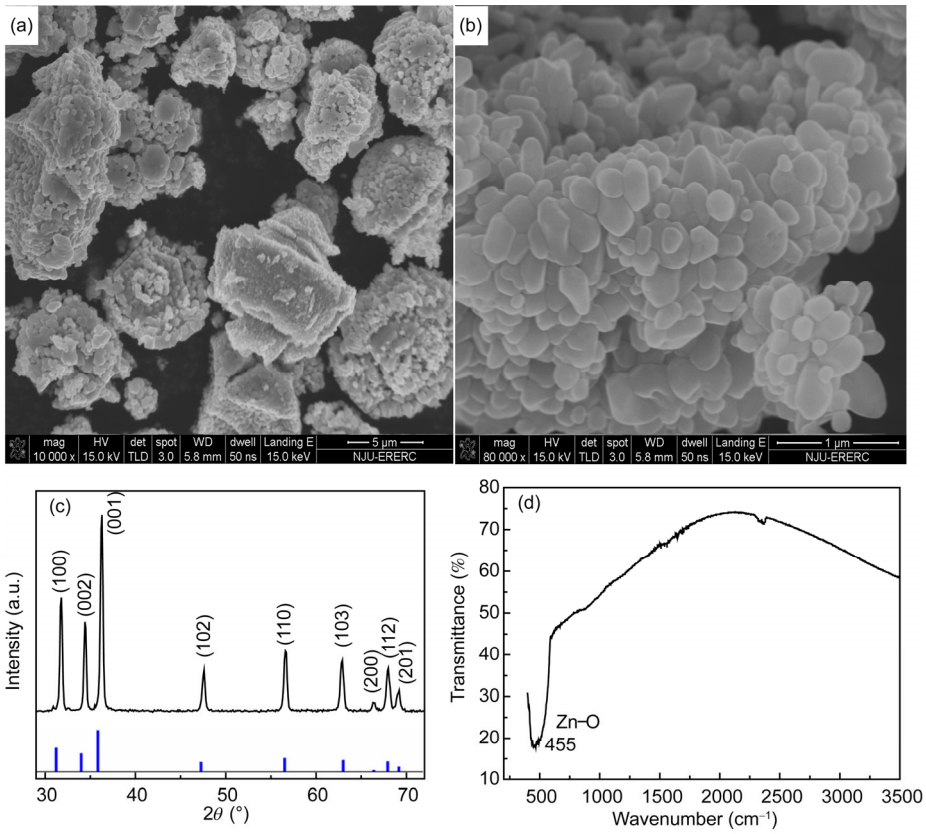

Figure 2 SEM images (a, b), XRD pattern (c) and FT-IR curve (d) of obtained ZnO NPs.

There is only one intense peak at 455 cm^{-1} associated with the characteristic stretching vibration mode of Zn–O bonding [17]. The absorption peaks observed between 2300 and 2400 cm^{-1} are from the existence of CO_2 molecule in air. The absence of absorption peak at ca. 3400 cm^{-1}, usually coming from normal polymeric O–H stretching vibration of H_2O, discloses that ZnO NPs adsorb less water vapor and have less porous structure and small surface area. Less porous structure and small surface area of the product are also helpful to inhibit photocorrosion [9–13]. So, the results reflected from SEM, XRD, and FT-IR support ZnO NPs as an excellent photocatalyst.

3.1.2 TEM, HRTEM images, and EDX pattern

A little ZnO NPs were dispersed in ethanol under ultrasonic condition for 30 min, and a droplet of suspension was dripped onto copper grids coated with ultrathin carbon film. Thus TEM operation was undertaken and TEM image is shown in Figure 3(a). It is seen that, the ZnO NPs obtained have a mean diameter in size of ca. 100–150 nm and are monodispersed in ethanol after ultrasonic treatment. The irregular hexagonal morphologies of ZnO particles are clearly seen (indicated by red circles), consistent with the previous reports that nonlayered compounds with hexagonal phase are inclined to the formation of hexagonal cross sections in the high reactant concentrations [18,19]. It was reported that hexagonal platelike ZnO had much positive effect on its photocatalytic activity because larger polar faces at hexagonal platelike ZnO surface were present [20]. A ripplelike contrast observed in the TEM image is due to the strain-stress in ZnO NPs [21]. Inset in Figure 3(a) is a selected area electron diffraction (SAED) pattern, indicating single crystal structure and very high crystalline degree of the product. EDX pattern shows Zn, O, and Cu elements; thereof the atomic ratio of Zn to O is 37.95:38.80, approaching 1:1, and the Cu element is from the Cu grids. There are no mesopores in every ZnO nanoparticle. The HRTEM images (Figure 3(c, d)) show distinct particles with well-defined crystalline boundaries resulting from highly crystallized material. The spacing of 4.93 Å between adjacent fringes corresponds to the *d*-spacing of (101) planes in hexagonal ZnO. The highly crystalline degree of the product is helpful in preventing itself from photocorrosion [10]. Also, there are high densities of stacking faults on (101) planes, suggesting as-prepared product might be an excellent photocatalyst [8].

3.2 BET surface area of the photocatalyst

Surface area and pore structure of the photocatalyst are directly related to its photocatalytic activity. Figure 4 shows the corresponding nitrogen adsorption/desorption isotherms

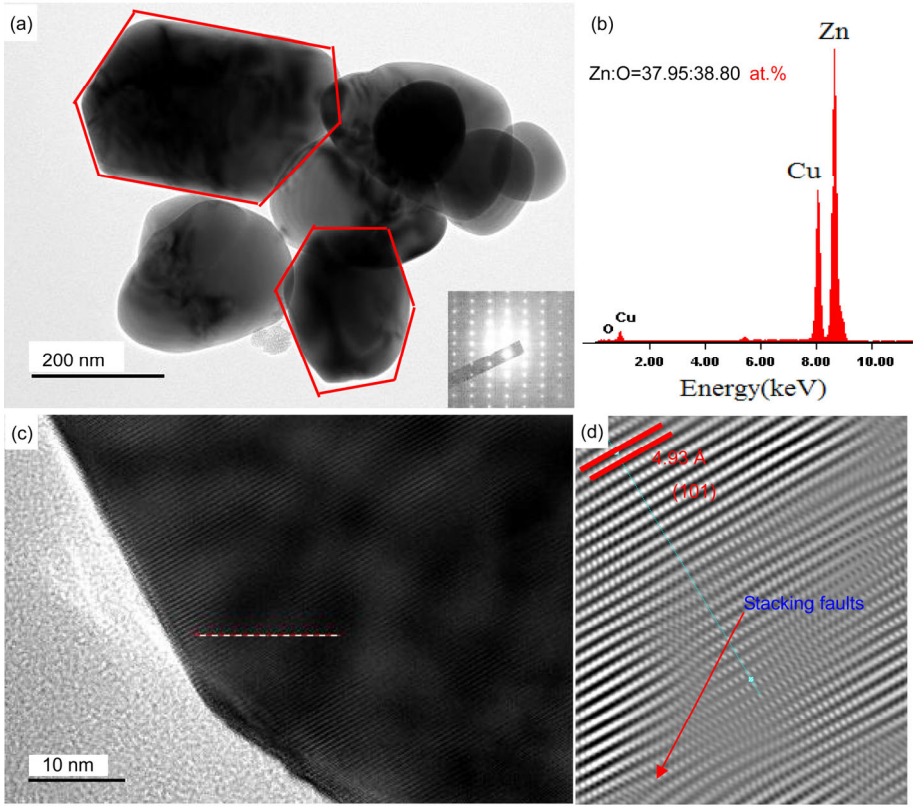

Figure 3 TEM image (a), EDX pattern (b), HRTEM image (c), and the corresponding Fourier transform (d) of obtained ZnO NPs. Inset of (a) is a SAED pattern.

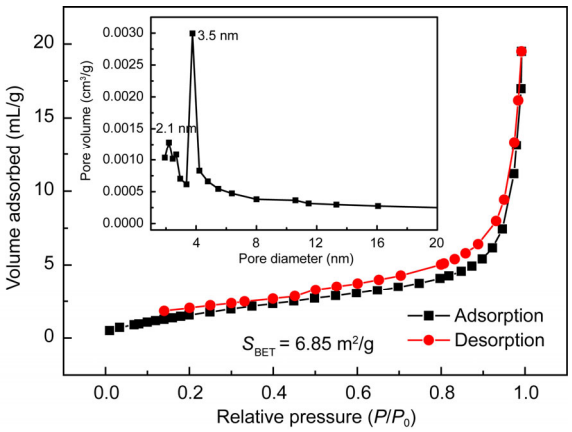

Figure 4 Nitrogen adsorption-desorption isotherm and BJH pore-size distribution plot (insert) of the as-prepared ZnO NPs.

and Barrett-Joyner-Halenda (BJH) pore-size distribution curve of the ZnO NPs. These isotherms belong to Type IV H3 loops of the ZnO NPs comprising aggregates of nanoparticles forming slit-like mesopores [22]. The pores with 2.1 and 3.5 nm are from the interstices between ZnO nanoparticles. The examined BET surface area of the ZnO product is 6.85 m^2/g. On the other hand, the surface area of the product can be theoretically expressed by the formula $S_{BET}=6000/d\rho$ (where ρ is the density of ZnO with a value of 5.8, and d is its average diameter of ca. 100 nm as shown in Figure 3), since there is no porous hole for the approximately ball-shaped ZnO nanoparticles (Figure 3(a, c)). The calculated surface area of the prepared product is in the range of 6.9–10.3 m^2/g. Therefore, the actual surface area of the products might suggest a little conglomeration for the ZnO NPs powder, though showing monodisperse state for ZnO NPs in ethanol.

3.3 Optical properties of the photocatalyst

ZnO NPs were also investigated by Raman spectroscopy (Figure 5(a)). The peak at 434 cm^{-1} is attributed to ZnO nonpolar optical phonon high E_2 mode. The peak at 95 cm^{-1} is from its low E_2 vibration. The peak at 329 cm^{-1} is assigned to the second-order Raman spectrum arising from Brillouin zone boundary (M point) phonon 2-E2(M). The E_2 mode is usually used to analyze the stress state in films due to its high sensitivity to stress [23]. Compared with E_2 (high) mode of bulk ZnO (437 cm^{-1}), E_2 (high) peak of our sample shows red shift. Such a shift cannot be attributed to the quantum confinement effect of an optical phonon since all ZnO nanoparticles have radii larger than the bulk ZnO exciton Bohr radius (~2.34 nm). The frequency shift of the E_2 mode (high) may be attributed to the strain-stress in ZnO NPs (also reflected from TEM images in Figure 3), which allegedly resulted from more defects such as oxygen vacancy [24]. Oxygen vacancies in ZnO can act as potential wells to trap electrons, aiding electron-hole pair separation and hence increasing the photocatalytic activity [20]. The

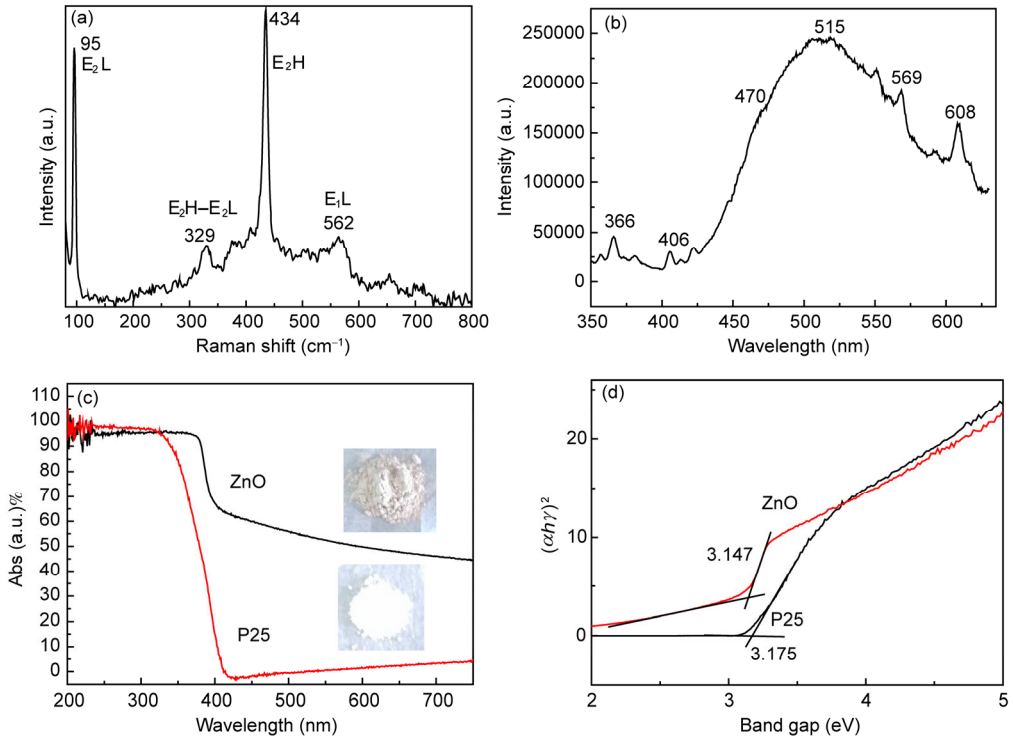

Figure 5 Raman (a), room-temperature photoluminescence (b), UV-Vis diffuse reflectance (c) spectra, and plots of $(\alpha h\gamma)^2$ vs. the energy of absorbed light (d) for the as-synthesized ZnO NPs. Insets of (c) are the corresponding photographs of ZnO NPs and P25.

strong E_2H peak and the weak E_1L peak reveal the high crystalline degree of ZnO NPs, agreeing with the examinations by XRD, FT-IR, and HRTEM. The peak at 562 cm^{-1}, usually attributed to the E_1L mode, is caused by the oxygen vacancy, zinc interstitial, or their complexes. As known, the oxygen vacancy in ZnO would sensitively influence the luminescence properties. ZnO NPs are further evaluated by room-temperature PL spectra, as shown in Figure 5(b). The weak UV emission at ~366 nm corresponds to the near band edge (NBE) emission. The violet emission at 406 nm is commonly attributed to the oxygen dangling bonds on the glass surface or the interface between glass substrate and ZnO nanostructures (Note: ZnO NPs were placed on glass substrate when operating PL spectrum experiment) [25]. The blue luminescence at 470 nm could be attributed to zinc vacancy. The green emission, centered at 515 nm in the range of 500–570 nm, was said to be from the recombination of electrons with holes trapped in singly ionized oxygen vacancies (V_O^+) and is commonly seen in ZnO materials synthesized under oxygen-deficient conditions [26]. The orange emission centered at 608 nm can be attributed to only oxygen interstitials. The large ratio of green PL intensity to NBE PL intensity indicates that the as-grown ZnO NPs are indeed rich in atomic defects (oxygen vacancies), which might result in high densities of stacking faults in ZnO NPs (Figure 3(d)), and help to enhance the photocatalytic activity [20].

Figure 5(c, d) shows UV-Vis diffuse reflectance spectra of ZnO NPs and the referenced P25. It is seen that the ZnO NPs have a wider absorption in the UV range than P25. So, the prepared ZnO NPs can use fully the most UV light in sunlight than P25, suggesting that the ZnO NPs would be a more ideal photocatalyst under the solar light irradiation. There is an asymmetric tail toward the higher wavelengths ranging from 400 to 700 nm in ZnO NPs, just because of the colored product (dust gray, see photographs of ZnO NPs and P25, insets in Figure 5(c)). The plot of $(\alpha h\gamma)^2$ vs. the energy of absorbed light shows the direct allowed band gaps of ZnO NPs and P25 are 3.147 and 3.175 eV, respectively. The absorption edges of ZnO are red-shifted (bulk ZnO, 3.36 eV) probably due to the increased intra-stress in particles (also proved by TEM images in Figure 3(a) and Raman spectrum in Figure 5(a)) [16].

3.4 Photocatalytic activity of ZnO NPs and their recycle

3.4.1 Photocatalytic degradation of RhB over ZnO NPs and P25 under solar light and UV irradiation

Photocatalytic activity of ZnO NPs was tested by the degradation of RhB under solar light/UV irradiation, and P25 was also evaluated under the same photocatalytic condition for comparison. As shown in Figure 6, the degradation ratio of RhB was almost 100% over the ZnO NPs in 40 min under solar light irradiation, and it is ca. 90% for P25. The

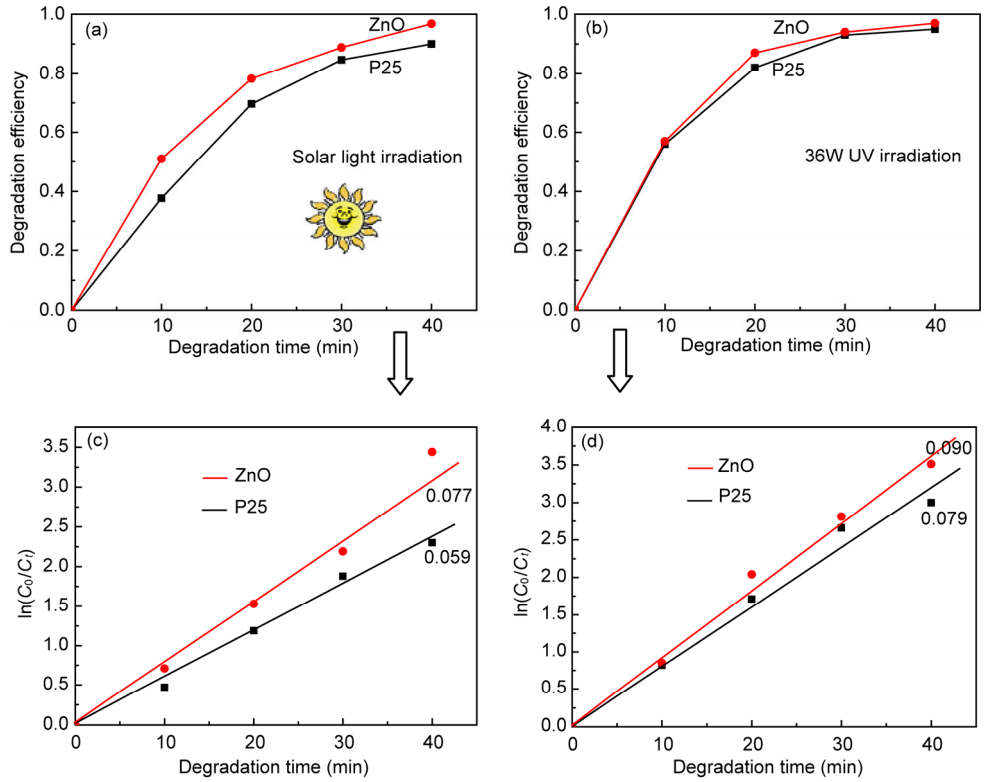

Figure 6 Degradation ratio of Rh-B over ZnO NPs and P25 photocatalysts under solar light (a) and UV (b) irradiation for different times and corresponding kinetic study (c, d).

better photocatalytic activity of ZnO NPs than P25 is attributed to their full absorbance of sunlight wave-band due to their dust gray. Under UV (36 W) irradiation, the ZnO NPs also showed comparative photocatalytic activity to P25. Importantly, the solar catalytic activity of ZnO NPs is comparative to the UV catalytic activity, suggesting their practical application in wastewater. The reaction kinetics was further depicted by the curve of $\ln(C_0/C)$ to reaction time t, and pseudo-first-order reaction could be inferred. The reaction rate constant (denoted as k) over ZnO NPs (0.077 for solar light and 0.09 for UV) is a little higher than over P25 (0.059 for solar light and 0.079 for UV). Compared with our previous ZnO NPs (the full degradation of RhB needs the time of 4 h) [16], the prepared ZnO NPs in this study show far better photocatalystic activity (the full degradation time is 40 min), just due to much better crystalline degree (Figures S2–S4). Therefore, the highly crystalline degree of the product plays an important role in enhancing the photocatalytic activity. In general, the enhanced photocatalytic activities of ZnO NPs can be mainly attributed to such facts as high crystalline degree (proved by XRD pattern, HRTEM image, and SAED pattern), having less mesopores (from the FT-IR curve and TEM images), large size of nanoparticles (seen in TEM image), and plenty of stacking faults (revealed by HRTEM image, BET curve, Raman, and PL spectrum), which could prevent the photocorrosion of the product and provide enough high-energy reaction sites for photochemical reaction [9–13]. Therefore, the wide band light and photogenerated electrons and holes would be used much more efficiently in the photocatalytic reaction, thus improving the quantum efficiency.

3.4.2 The recycle of ZnO NPs

The convenient reuse of photocatalysts is essential to their practical applications in purifying wastewater. After completing every photocatalystic test, the top degraded solution was poured out quickly, and 35 mL of RhB solution was added to the quartz cup again for the next photocatalytic test. Figure 7 shows the reusability of ZnO NPs and P25 photocatalysts for the photocatalytic degradation of RhB under UV light (36 W) irradiation. It is noted that ZnO NPs powder has good reusing capacity; even though the reuse time number reached 4, the degradation ratio of RhB is still as high as ca. 80% in 40 min. The excellent self-recycled ability of ZnO NPs is due to large size, heavy density (5.8 m/mL), and small surface area of ZnO NPs (see TEM images and BET curve), which help in the quick self-precipitation of ZnO NPs in water [16]. In contrast, P25, a most extensively used commercial photocatalyst, had bad recovery ratio as low as less than 10% after several times of recycling due to the small size and porous structure [16]. Through the comparative test of reuse of photocatalysts, the ZnO NPs in this study have a practical application in purifying wastewater.

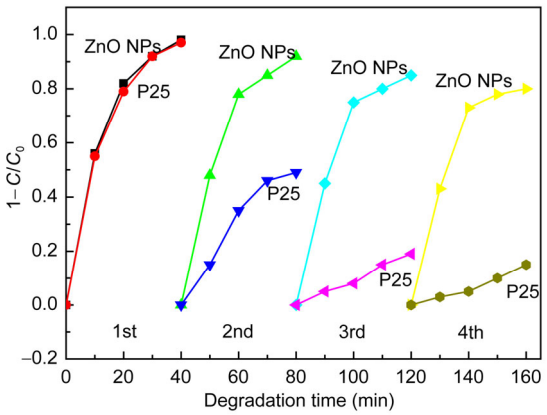

Figure 7 Reusability of ZnO-NPs and P25 photocatalysts for the photocatalytic degradation of RhB under UV light (36 W) irradiation.

4 Conclusions

ZnO NPs were harvested via the reaction of Zn powder with H_2O vapor in autoclave. After systematic characterizations, the ZnO NPs composed of hexagonal platelike nanoparticles showed high crystalline degree, large size of 100–150 nm in diameter, small BET surface area of 6.85 m^2/g, a little red-shift as a comparison with bulk ZnO band gap because of the existence of strain-stress in ZnO NPs, and had a strong green emission due to plenty of atomic defects. The obtained ZnO NPs showed excellent photocatalytic activity on the degradation of RhB under solar light irradiation, and repetitious recycle due to their quick sedimentation in water. Therefore, the ZnO NPs prepared from Zn powder have a wide and promising application in purifying the wastewater.

Acknowledgments We are grateful to Dr. Guoqiang Jian in University of Maryland for the help of HR-TEM. This work was supported by the National Natural Science Foundation of China (21161016), the Natural Science Foundation of Jiangxi Province (20142BAB216013), Jiangxi Education Department Fund (KJLD14087, GJJ14714) and Jiangxi Environmental Protection Department Fund ([2013]370).

Conflict of interest The authors declare that they have no conflict of interest.

Supporting information The supporting information is available online at http://chem.scichina.com and http://link.springer.com/journal/11426. The supporting materials are published as submitted, without typesetting or editing. The responsibility for scientific accuracy and content remains entirely with the authors.

1 Khin MM, Nair AS, Babu V, Murugan R, Ramakrishna S. *Energy Environ Sci*, 2012, 5: 8075–8109
2 Chan SHS, Wu TY, Juan JC, Teh CY. *J Chem Tech Biotech*, 2011, 86: 1130–1158
3 Ullah I, Ali S, Hanif MA, Shahid SA. *Intern J Chem Biochem Sci*, 2012, 2: 60–77
4 Zhang DQ, Li GS, Yu JC. Advanced photocatalytic nanomaterials for degrading pollutants and generating fuels by sunlight. In: Zhang L, Ed. *Energy Efficiency and Renewable Energy Through Nanotechnology*. London: Springer London, 2011. 679–716

5 Chen X, Mao SS. *Chem Rev*, 2007, 107: 2891–2959
6 Li Y, Zhou X, Hu X, Zhao X, Fang P. *J Phys Chem C*, 2009, 113: 16188–16192
7 Behnajady MA, Modirshahla N, Hamzavi R. *J Hazard Mater*, 2006, 133: 226–232
8 Xu LP, Hu YL, Pelligra C, Chen CH, Jin L, Huang H, Sithambaram S, Aindow M, Joesten R, Sui SL. *Chem Mater*, 2009, 21: 2875–2885
9 Meng SG, Li DZ, Zheng XZ, Wang JX, Chen J, Fang JL, Shao Y, Fu XZ. *J Mater Chem A*, 2013, 1: 2744–2747
10 Dijken AV, Janssen AH, M. Smitsmans HP, Vanmaekelbergh D, Meijerink A. *Chem Mater*, 1998, 10: 3513–3522
11 Pudukudy M, Hetieqa A, Yaakob Z. *Appl Surf Sci*, 2014, 319: 221–229
12 Meulenkamp EA. *J Phys Chem B*, 1998, 102: 7764–7769
13 Velmurugan R, Selvam K, Krishnakumar B, Swaminathan M. *Sep Purif Technol*, 2011, 80: 119–124
14 Subash B, Krishnakumar B, Swaminathan M, Shanthi M. *Langmuir*, 2013, 29: 939–949
15 Tan TV, Río Ld, Valdés-Solís T, Marbán G. *Appl Catal B*: *Environ*, 2013, 140–141: 189–198
16 Lv YY, Yu LS, Huang HY, Feng YY, Chen DZ, Xie X. *Nanotechnology*, 2012, 23: 065402–065409
17 Perales-percz Q, Parra-palomino A, Singhal R, Voyles Y, Zhu Y, Jia W, Tomar MS. *Nanotechnology*, 2007, 18: 315606– 315611
18 Liu C, Hu Z, Wu Q, Wang XZ, Chen Y, Sang H, Zhu JM, Deng SZ, Xu NS. *J Am Chem Soc*, 2005, 127: 1318–1322
19 Chen X, Ma J, Hu Z, Wu Q, Chen Y. *J Am Chem Soc*, 2005, 127: 7982–7983
20 Mclaren A, Valdes-Solis T, Li GQ, Tsang SC. *J Am Chem Soc*, 2009, 131: 12540–12541
21 Pan ZW, Dai ZR, Wang ZL. *Science*, 2001, 291: 1947–1949
22 Kruk M, Jaroniec M. *Chem Mater*, 2001, 13: 3169–3183
23 Decremps F, Porres JP, Saitta AM, Chervin JC, Polian A. *Phys Rev B*, 2002, 65: 092101–092104
24 Zhang Y, Jia HB, Wang RM, Chen CP, Luo XP, Yu DP, Lee C. *Appl Phys Lett*, 2003, 83: 4631–4633
25 Teng XM, Fan HT, Pan SS, Ye C, Li GH. *J Phys D*: *Appl Phys*, 2006, 39: 471–476
26 Greene LE, Law M, Goldberger J, Kim F, Johnson JC, Zhang YFR, Saykally J, Yang PD. *Angew Chem Int Ed*, 2003, 42: 3031–3034